International Journal of Civil Engineering
https://doi.org/10.1007/s40999-019-00482-7

RESEARCH PAPER

Flows of Liquefied Filtered Tailings: Laboratory-Scale Physical and Numerical Modeling

John A. Sánchez-Peralta[1] · Lorena N. Beltrán-Rodríguez[1] · Mario G. Trujillo-Vela[1] · Joan M. Larrahondo[1]

Received: 12 June 2019 / Revised: 23 September 2019 / Accepted: 30 October 2019

Abstract

The numerical prediction of the runout and spread of liquefied-tailings flows is a complex problem that depends on many factors, including the rheological properties of the liquefied tailings. However, published benchmark problems specific to tailings flows, useful for validation and calibration of numerical models, are virtually nonexistent. This paper presents a laboratory-scale benchmark problem of liquefied-tailings flow. Gold filtered tailings were characterized via rheological measurements, geotechnical index tests, and toxicity chemical analysis. Physical flow experiments of the liquefied-tailings paste, at 70% solids concentration, were carried out in an instrumented laboratory flume with high-speed video and direct measurements of the at-rest "footprint" (lobe) dimensions. Subsequently, using the measured physical parameters, computational fluid dynamics (CFD) tools were used to solve the three-dimensional, rheology-dependent Navier–Stokes equations via the finite-volume method and a multiphase volume-of-fluid (VOF) technique. Thus, the at-rest lobe of the spilled tailings was numerically reproduced. Results show that the liquefied tailings bear nearly zero-yield stress and low viscosity, thereby practically behaving as a Newtonian fluid despite their high solid concentration. In addition, good agreement (within 14% of the main dimensions) was found between the physical and numerically simulated at-rest lobes. Hence, the use of a Navier–Stokes approach, supported on a finite-volume/VOF technique, and a Newtonian-fluid constitutive rheological model, simulates well the at-rest shape of liquefied tailings at laboratory scale. This benchmark problem will aid numerical research specific to tailings flows.

Keywords Filtered tailings · Rheology · Viscosity · Benchmark problem · Computational fluid dynamics · Finite-volume method

1 Introduction

Tailings storage facilities (TSFs), widely used in the mining industry, are normally built to retain millions of cubic meters of mine waste [1, 2]. Most TSFs are complex geotechnical structures, because the embankment height is sequentially risen throughout the mining project's life; also, the embankment body is frequently formed with the coarse fraction of the mine waste itself, and TSF post-closure costs are high [2]. Failures of TSFs have been attributed to a wide variety of causes, including overtopping, slope instability, seismically induced liquefaction, foundation instability, mine subsidence, rain intensity, snow thawing, pond water management, and piping [2–4].

According to the International Commission on Large Dams [5], the probability of failure of TSF structures is about 100 times greater than that of water retention dams. Others estimate the latter factor as ten times, representing about two significant failures per year [6]. During the twentieth century, 250 cases of tailings dam failures were compiled worldwide [2], although it is uncertain how many cases have been unreported. Historical TSF failures with runouts in the scale of tens of kilometers (e.g., Aznalcóllar, Spain, 1998 [1, 7–12] and Merriespruit, South Africa, 1994

John A. Sánchez-Peralta: Deceased.

✉ Joan M. Larrahondo
jlarrahondo@javeriana.edu.co

Lorena N. Beltrán-Rodríguez
lorena.beltran@javeriana.edu.co

Mario G. Trujillo-Vela
mario.trujillo@javeriana.edu.co

[1] Department of Civil Engineering, School of Engineering, Pontificia Universidad Javeriana, Edificio No. 42, Oficina 18, Bogotá, Colombia

Published online: 28 November 2019

[13]), as well as recent catastrophic disasters (e.g., the Fundão, 2015 [14, 15] and Brumadinho, 2019 dam failures in Brazil), highlight the profound social, environmental, and economic consequences of tailings spill disasters [3, 16].

The quantitative analysis of the behavior and runout of tailings flows demands consideration of many factors, including type of TSF, the likely failure mechanism, and local topography. In addition, the study of tailings flows requires accounting for the rheological properties of the liquefied material [17–20], particularly the solid content-dependent yield stress and the strain-rate-dependent viscosity. The analysis of the rheological behavior of tailings also has implications on pipeline design and performance of slurry pumping systems [21].

Computational fluid dynamics (CFD) is a powerful tool to solve the mass and momentum conservation equations of flow while accounting for its rheological properties [22]. CFD tools have aided the study of an ample group of Newtonian and non-Newtonian flows, including tailings [18, 20, 23]. Unfortunately, while published benchmark problems useful for validation and calibration of CFD simulations are widely available in the literature (e.g., [24, 25]), published benchmark problems specific to liquefied-tailings flows are virtually nonexistent. In fact, benchmark problems in tailings research are currently limited to chemical reactive transport phenomena, particularly acid rock drainage attenuation and uranium bioremediation [26, 27].

This article introduces a laboratory-scale benchmark case of liquefied-tailings flow. First, the spread of a filtered-tailings liquefied paste that flows upon controlled sudden-release conditions is physically monitored in the laboratory. Subsequently, computational fluid dynamics (CFD) tools are used to solve the three-dimensional rheology-dependent Navier–Stokes equations to replicate the at-rest "footprint" shape of the spilled tailings. This benchmark problem is simple though meaningful and is intended to aid numerical research on tailings flows.

In this paper, the term "liquefied tailings" refers to the physical state attainable by contractive, strain-softening tailings once they are subjected to shear under undrained conditions, e.g., after their containment barrier breaks [3, 6, 12]. Under such conditions, positive pore water pressures build up and the tailings liquefy. This behavior resembles that of "flow liquefaction" or "static liquefaction" after the monotonic stress path of a contractive, strain-softening soil crosses a "phase transformation line" [28]. In this context, liquefied shear strength is "the shear strength mobilized at large deformation by a saturated contractive soil following the triggering of a strain-softening response." [29] Because the physical experiments presented in this paper use contractive tailings that are subjected to laboratory-scale sudden-release conditions (resembling those of a dam break), the material that flows can be treated as "liquefied tailings".

2 Background

2.1 Physical and Numerical Modeling of Tailings Flows

Previous studies on empirical modeling of tailings flows include those by Rico and Lucia and Duncan [2, 30]. Based on historical reviews of tailings dam failures, those researchers propose correlations to estimate post-failure flow runout depending on the dam geometry and the volume or height of the contained waste.

In the field of saturated granular tailings, other researchers have implemented a brittleness index to assess the susceptibility of iron, zinc, and garnet tailings to trigger rapid flow slides under monotonic, incremental loading [31] (the brittleness index depends strongly on initial void ratio, as well as on undrained peak and residual strength). A different group of studies [32–34] present tailings-flow models assuming that their behavior is similar to that of slope or debris motion.

More recently, experimental and numerical studies have addressed flows of varying viscosity in the laboratory [20, 23], and use CFD simulations to solve the corresponding mass and momentum conservation equations. CFD techniques have also been implemented in infrastructure performance assessment of tailings-pumping systems as well as in the analyses of tailings beach spreading [18, 35, 36]. Rheological properties of tailings suspensions have been determined elsewhere for conventional tailings [37] as well as for cemented paste backfill (CPB) [38].

Regarding flows of non-tailings waste materials, e.g., municipal solid waste, physical modeling has focused on monitoring runout, at-rest footprint shape, flow depth, velocity, and angle of reach of moist soil simulants [39]. In addition, other physical/numerical modeling efforts have focused on post-liquefaction soil flows using two-dimensional CFD tools and model-box experimental validation, while assuming that the liquefied soil behaves as a viscous fluid [40].

2.2 Theoretical Framework

The Navier–Stokes equations assume the flow as a continuum that is characterized by density (ρ), dynamic viscosity (μ), pressure (P), and velocities (u, υ, ω), through time (t) [22].

The three-dimensional conservation of mass, considering the fluid mass balance in an infinitesimal control volume, establishes that the rate of mass increase equals the gradient of mass flow rate across the volume:

$$\frac{\partial \rho}{\partial t} = -\rho \nabla \cdot \mathbf{u}, \quad (1)$$

where $\mathbf{u}$ is the three-dimensional velocity vector. When the fluid is assumed incompressible, the mass conservation equation is reduced to: $\nabla \cdot \mathbf{u} = 0$.

On the other hand, the three-dimensional conservation of momentum indicates that the rate of change of momentum per unit volume equals the sum of all fluid forces, i.e., inertial, pressure, body, and viscous forces:

$$\rho \frac{\partial \mathbf{u}}{\partial t} = \rho (\mathbf{u} \cdot \nabla)\mathbf{u} - \nabla P + \rho S + \mu \nabla^2 \mathbf{u}, \quad (2)$$

where S represents the body forces in the x-, y-, and z-directions.

Finally, conservation of energy must also be satisfied. Nonetheless, this research assumes that no heat or entropy variations take place during the liquefied-tailings flows.

The partial differential equations representing flows of debris, mud, avalanches, and tailings can be approximated by various spatial and temporal discretization techniques, including the finite-difference, finite-volume, and finite-element methods [33, 41].

Fig. 1 Filtered tailings used in this study. **a** Tailings dewatering system: compressing plates with cloth filters and air injection; **b** pile of low water-content tailings cake produced by the tailings dewatering system

3 Materials and Methods

The tailings used in this investigation were kindly provided by an active mining project located in the region of Antioquia, Colombia, which to date is the first in the country to use filter-dewatering technology. By circulating the process-water tailings suspension through a series of cloth filters compressed by vertical plates (see Fig. 1a), followed by in-filter air injection at high pressure, this technology allows for significant reductions in the water content of the tailings. The final product of this process is a "cake" of low water content (around 20%) that is gradually piled up by the filtering-plant site (see Fig. 1b). The reclaimed water is reused during the ore-extraction process of the mineral, while the tailings cake is disposed of by conventional engineered-embankment compaction.

3.1 Tailings Properties

At the mining project, the samples were collected in 15 plastic buckets, about 20 L each, which were manually filled with filtered-tailings cake pieces.

Prior to handling and characterizing the tailings in the laboratory, the possible presence and concentration of heavy metals in the tailings were determined in a commercial laboratory (Chemilab SAS, Bogotá, Colombia) via the toxicity characteristic leaching procedure (TCLP), according to the EPA standard No. 1311 [42]. Then, fundamental index properties of the tailings were determined (see Table 1).

The rheological properties of the liquefied-tailings pastes were measured with a Brookfield DV-III Ultra programmable viscometer (Brookfield Engineering Laboratories Inc., Massachusetts, USA). The measuring range of the instrument is determined by the speed of rotation, the size and shape of the spindle, and the container in which it rotates [43]. Segregation of the samples was prevented via thorough manual mixing in the testing container prior to performing the measurements. The same instrument type has been recently used by others in cemented paste backfill (CPB) research to determine rheological yield stress at high solid contents [38].

After performing a series of preliminary tests, the spindles No. SC4-21 and SC4-27 were selected out of the 11 spindles available with the Brookfield DV-III Ultra device (RV and SC4 series). The remaining spindles yielded no measurable shear-stress values or the range of working viscosities was outside that of the liquefied

Table 1 Index tests performed in the tailings

Test	Method	Number of tests
Water content (as received)	ASTM D2216	5
Tailings-paste density	API RP13B-1	5
Specific gravity	ASTM D854	5
Grain-size distribution (washed over sieve #200)	ASTM C136-01	5
Grain-size distribution (hydrometer)	ASTM D422	5
Liquid limit (Casagrande cup)	ASTM D4318	5
Liquid limit (fall cone)	BS 1377:1990	5
Plastic limit (rolls method)	ASTM D4318	5
pH (supernatant)	–	3
pH (paste)	–	3

tailings. In total, 86 shear-strain-rate controlled measurements of shear-stress vs. shear-strain rate were obtained during this study.

3.2 Physical Experiments

3.2.1 Preliminary Experiments

To define the spatial scale of the tailings-flow experiments, eight preliminary flow tests were conducted. For these tests, tailings-paste volumes were 0.6 L (three experiments), 2.5 L (three experiments), and 15 L (two experiments). During the first two sets of tests, the tailings were first air dried during 24 h, then macerated on a hand mortar, and finally homogenized with a jar test during 1 h at 120 rpm. For the third set, the tailings were first air dried during 24 h, then macerated in the Los Angeles machine, and finally mixed in a 150-L capacity portable concrete mixer. The eight preliminary tests included varying concentration of solids between 60 and 71%, and flow surfaces of aluminum sloping between zero and 10% (Fig. 2).

The largest at-rest "footprint" of these preliminary flow experiments yielded 1.4 m in length and 0.66 in of width, using 15 L of tailings paste, 60% of solid concentration, and zero-sloping surface. Based on the preliminary tests, Sect. 3.2.2 describes that the experimental conditions adopted for the final benchmark tests were 27 L of tailings-paste volume, 70% concentration of solids, and flat aluminum surface. These conditions guaranteed that the final lobe (footprint) of the benchmark experiments would fit into the testing flume available.

3.2.2 Tailings-Flow Benchmark Experiments

Similar to the preliminary experiments, liquefied tailings were prepared as suspensions of dry tailings in water, which were homogenized with a jar test during 1 h at 120 rpm, and then allowed to settle under gravity for 24 h. After sedimentation, the measured concentration of solids was 70% in weight. This value was subsequently used to design the spill system, the flow monitoring system, and the amounts of tailings and water to be employed.

For the experimental stage, the environmental flume for slope simulations located in the Geotechnical Laboratory of Pontificia Universidad Javeriana was used (Fig. 3); the flume is described in detail elsewhere [44]. The dimensions of the flume are 3-m long by 1-m wide.

A container was constructed to produce a controlled, sudden spill (Fig. 4). The container was 50 cm in height and 30 cm × 30 cm at the base; the container was built with acrylic sheet of 3 mm in thickness. On one of the sides, a 40-cm × 10-cm gate was provided, which opened manually via a metal pulley. The outer edges of the container were reinforced with steel sheet. A 130-cm-long by 68-cm-wide, flat aluminum sheet was placed at zero-degree

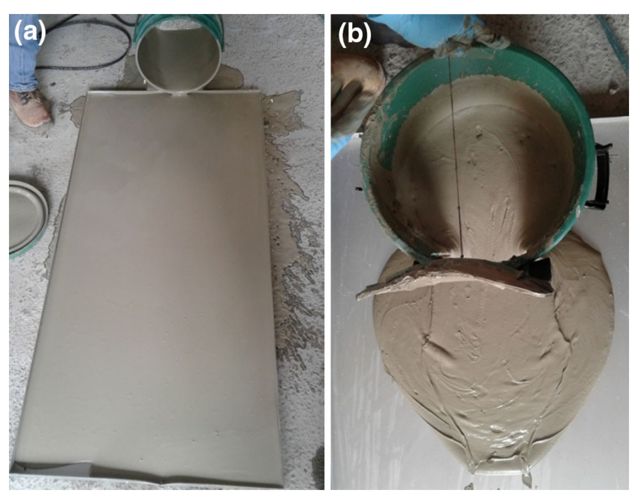

Fig. 2 Preliminary physical experiments: 15 L of tailings paste spilled on a flat aluminum surface. **a** 60% solid concentration; **b** 70% solid concentration

(0°) slope to provide a homogeneous low-roughness travel surface for the flow.

The tailings to be tested were randomly sampled and placed in an oven for 24 h at 110 °C to control the exact amount of water to be added at the time of preparing the liquefied tailings. Afterwards, the dry tailings were macerated using the Los Angeles machine (about 12 kg in a cycle of 100 turns) to remove lumps and to be able to work with loose material.

For each experiment replicate, 35 kg of dry tailings and 15 kg of tap water were mixed in a portable concrete mixer to attain the target weight concentration of 70% that was determined previously in the laboratory. Finally, from the prepared tailings, 27 L were recovered to run each experiment. This volume was poured gently into the acrylic container and remained homogenized using a portable propeller mixer adapted to a hand drill (see Fig. 4) until the moment of running the experiment. The height of liquefied tailings (inside the acrylic container) was 30 cm for all experiments. In total, five experiments of controlled sudden-release were carried out to assess repeatability of results.

For monitoring the liquefied-tailings-flow patterns and at-rest state, a Sony PXW-X200 high-speed video camera installed by the flume's lateral wall was used, along with a Kino Flo BarFly® 400 soft lighting system with 1000-W tungsten tubes (see Fig. 5).

To obtain additional direct point measurements of the dimensions and thickness of the at-rest "footprint" (lobe) of the spilled tailings, a tape measure with millimetric reading was used. The depths were measured at three locations of the pattern (Fig. 6), along its main axis, namely: at the container gate (maximum thickness), 30 cm horizontally from the container gate, and at the end of the lobe. Immediately after each experiment replicate was completed, three specimens of the spilled liquefied tailings were collected, for which rheometric flow curves were measured with the viscometer device, as explained above (see Sect. 3.1).

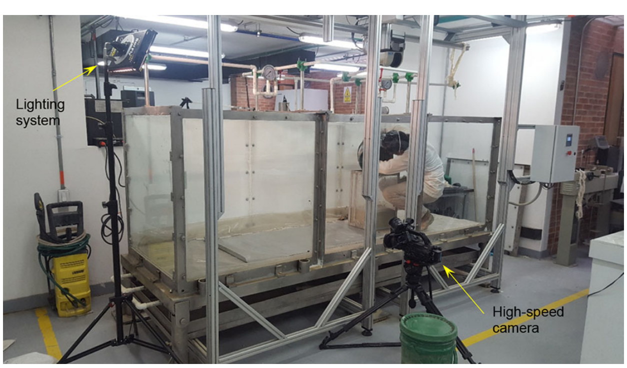

Fig. 3 Environmental flume for liquefied-tailings-flow experiments

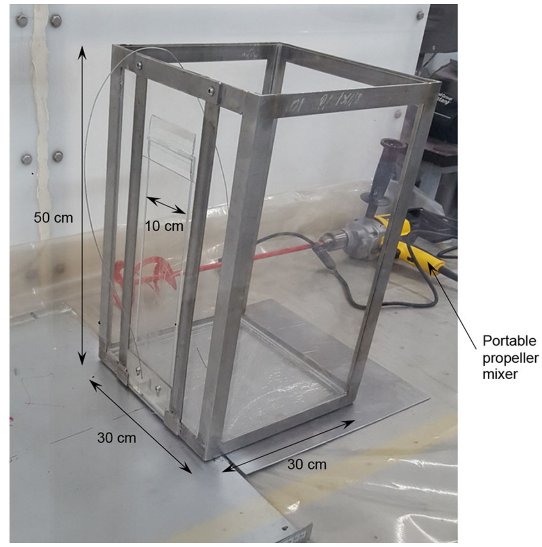

Fig. 4 Container, with manually operated gate, for the liquefied tailings

3.3 Numerical Experiments

In engineering, there are various models available for flow analysis due to dam breach, each with different capacities and levels of complexity. Some models simulate two or three dimensions, while others are only capable of dealing with one-dimensional flows. Most computational tools simulate Newtonian fluids (e.g., HEC-RAS and HEC-HMS), and a few others work with non-Newtonian flows (e.g., DAN-W, FLO-2D, and FLOW3D) [45]. For reasons of scale of the physical experiments, level of detail in the modeling, and capabilities of the software, Ansys® Fluent was selected for this research as the computational tool. Ansys® Fluent is a well-known tool that uses the approximation method of finite volumes with center in each cell, whereby the flow variables are stored in the centers of the volumes of the mesh [46–48].

Ansys® Fluent solves the equations of conservation of mass and momentum using a technique based on control volume, which includes: (1) dividing the domain into discrete control volumes using a computational grid; (2) integrating the governing equations in the individual control volumes, and thereby constructing algebraic equations with discrete dependent variables (unknowns) such as velocity, pressure, and temperature; (3) linearizing the discretized equations and solving the resulting system of linear equations to obtain updated values of the dependent variables.

In this research, a multiphase volume-of-fluid method (VOF) was employed, which is a free-surface tracking technique applied to a fixed mesh designed for two or more immiscible fluids, given that the position of the interface between the fluids is of interest. In the VOF method, the fluids share a single set of momentum equations and the volume fraction of each fluid in each computational cell is tracked throughout the domain. Thus, the selected primary phase was air, which occupies the largest portion of volume of the model, and the secondary phase was the liquefied tailings.

The geometry and meshing of the computational domain were defined from the "Workbench" interface of the program. The mesh was of unstructured automatic type with cubic cells of 2-cm side length. Mesh-independence tests were performed with cells of 5, 3, 2, 1, and 0.5-cm side lengths; it was concluded that, for meshes of 2, 1, and 0.5 cm, the results did not differ more than 1% in terms of resulting flow length and width. The mesh of 2-cm resolution was then selected as the optimum mesh, being the finest to achieve a good level of detail in the results and, simultaneously, the coarsest to save computational time (see Fig. 7).

The container from which the tailings flow was released was also included within the model geometry, specifically the 10-cm-wide gate from the physical experiments (see Fig. 7). Around the region of the container gate, the mesh was refined to 1-cm size. Overall, computational running times were close to 12 h per simulation.

Due to the mesh size, the released flow rate was very high at the beginning, and hence, Froude numbers exceeded the program's capacity of 250, and the computation was aborted in less than half of the final time. Therefore, it was necessary to decrease the time-step interval of the calculations to 0.0001 s.

The boundary conditions adopted for the base and walls of the numerical flume were "wall"-type boundaries in non-slip condition. Under these conditions, when the flow approaches any wall, it acquires a velocity equal to the wall's velocity. For the modeling, a stationary wall with zero velocity was used.

The numerical solution scheme adopted was a PISO algorithm type. Thus, pressure and velocity values during the non-iterative calculation of unstable compressible flows were determined. With this method, the interaction of a predictor step and two corrective steps that increase the accuracy of the results was implemented.

Finally, the input parameters for the liquefied tailings were swept between densities of 1400 to 1800 kg/m^3 and Newtonian-fluid viscosities of 1.79 to 3.07 Pa s. These parameters span above and below the experimentally measured values (see Sect. 4 for details). That is, the parameters adopted for the numerical simulations matched those measured during the physical experiments. No surface-tension considerations were made for the at-rest lobe during the analyses.

To check the numerical results with respect to mass conservation, the volume of the spilled lobe at the end of the simulations was compared against the initial volume. The results obtained by extracting the volume fraction of each phase (i.e., air and liquefied tailings) for each cell showed that the differences in mass were within ± 2%.

4 Results and Discussion

4.1 Tailings Properties

4.1.1 Index Properties

TCLP results indicate that the concentrations of heavy metals in the tailings are below the limit of detection, except for arsenic. However, the measured arsenic concentration is 0.0042 mg As/L, which is well below the maximum concentration for toxicity of 5 mg As/L, as established by the EPA [49]. The measured pH values are 8.09 (coefficient of variation CV = 0.63%) for the liquefied-tailings paste, and 7.93 (CV = 0.32%) for the supernatant sitting above a fresh paste. In both cases, the results showed a slightly alkaline aqueous solution.

During the handling of the tailings samples for liquid limit testing, despite their plasticity, segregation was observed in the wet mass of tailings, such that a film of water appeared rapidly above the mineral fraction. Because of the latter reason, and because the tailings were always handled wearing nitrile gloves, performing the plastic limit tests (rolls method) was extremely difficult.

The water content of the tailings, as received from the filtering-plant site, is 21.7% on average (CV = 1.4%). On the other hand, the equivalent gravimetric water content in the prepared liquefied tailings (at 70% solids concentration) is 43%. The liquid limit results obtained with the fall-cone method show values 20% higher than those measured using the Casagrande cup (see Table 2).

The USCS geotechnical classification of the filtered tailings used in this research, based on the Casagrande cup results, is CL (low-plasticity clay). Grain-size distribution curves of the tailings (see Fig. 8) indicate that the sand-size fraction, mostly fine sand, is 23.7% (CV = 4.1%), the silt-size fraction is 73.4% (CV = 10.2%), and the clay-size fraction is approximately 2.9% (CV = 1.4%). Mean diameter D_{50} is 0.032 mm. For comparison, the mean

Table 2 Consistency limits measured in the tailings (average; CV in parenthesis)

Method	LL (%)	PL (%)	PI (%)
Casagrande cup	26.4 (2.3)	17.9 (38.6)	8.6 (15.2)
Fall cone	31.7 (3.9)		13.8 (14.3)

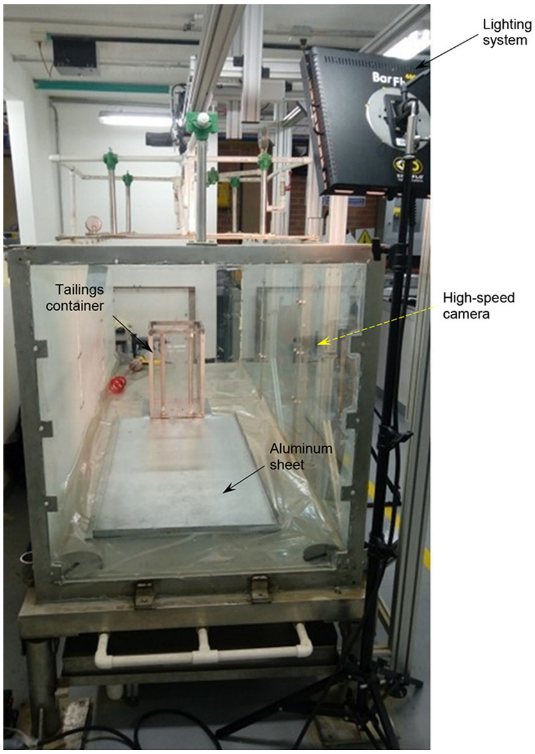

Fig. 5 Location of lighting and video camera for the benchmark experiments in the flume

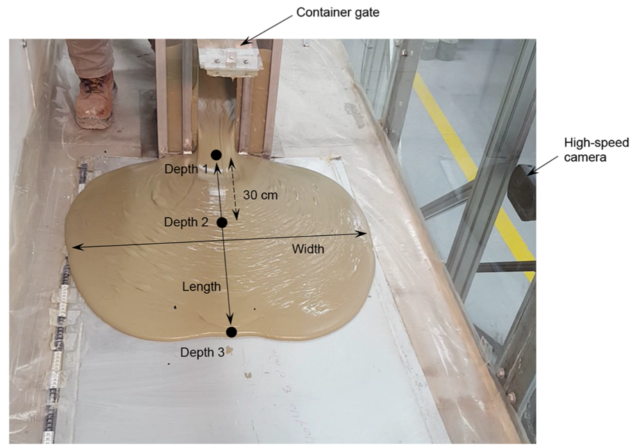

Fig. 6 Local-measurement points and dimensions on the spilled tailings at-rest lobes

diameter of conventional gold tailings at dam beaches typically ranges from 0.053 to 0.095 mm [50].

Interestingly, despite the fact that the dominant fraction is silt-sized, the USCS classification is clay. Considering that the tailings used in this study come from a filter-dewatering plant, the obtained grain-size distribution results suggest that the in-plant transit of the tailings through the filter press influences the grain-size distribution. That is, it is possible that the expelled water drags the clay-sized particles across the openings of the filter cloths and off the tailings mass. However, more data are required to confirm this observation.

The tailings' measured specific gravity is 2.77 on average (CV = 4.13%); for comparison, conventional gold tailings at dam beaches show specific gravities ranging from 2.69 to 3.20 [50]. Finally, the density of the liquefied-tailings pastes, as measured after gravity settling with a concentration of solids of 70%, is 1610 kg/m^3 (CV = 4.79%).

4.1.2 Rheological Properties

The rheometric results for the liquefied-tailings samples recovered immediately after each of the five benchmark spill experiments are presented in Fig. 9. Each flow curve in the figure corresponds to one separate benchmark experiment.

Best-fit analyses were performed considering three distinct rheological constitutive models. First, under the original assumption that the liquefied tailings would behave like a non-Newtonian fluid, a Bingham plastic-model fit (i.e., linear trend with positive vertical-axis intercept) was assessed. However, this fitting delivered negative values for the yield stress (− 4.77 to − 0.60 Pa).

Second, to evaluate whether the data would follow a dilatant or pseudo-plastic model, a power-law fit was used. This fitting yielded a correlation of R^2 = 0.92, with coefficient 1.92 (consistency index) and exponent 1.09 (behavioral index). The latter index represents the deviation of the rheological behavior from that of Newtonian fluids. In fact, if the behavioral index is greater than 1.0, the behavior is classified as dilatant; otherwise, it is pseudo-plastic. The resulting exponent indicates that the liquefied tailings of this study depict slightly dilatant behavior. However, with only 9% difference with respect to unity, these results suggest that the assumed non-Newtonian behavior of this material is not significant; that is, the behavior of the liquefied-tailings paste is practically Newtonian.

Finally, and based on the reasons above, the third attempt to fit the experimental data was linear again, though enforcing zero-yield stress; that is, a Newtonian rheological constitutive model, despite the relatively high solid content of 70%. The resulting average viscosity of the tailings is 2.55 Pa s if calculated averaging the five flow curves (see Fig. 9), or 2.62 Pa s if calculated using all the 86 measured data points from this study.

The cause for the virtually Newtonian response of the liquefied filtered tailings is still unclear, though the possible loss of clay fraction during in-plant filtering may be responsible (see Sect. 4.1.1), which would inhibit the development of yield stress. The absence of clay minerals in turn would prevent electro-chemical forces from developing within the tailings. As mentioned earlier, more research is required to confirm these statements.

4.2 Physical Experiments

The experimental results and local measurements of length, width, and thickness of the at-rest "footprint" (lobe) of the tailings flow produced after each benchmark experiment are presented in Table 3 and Fig. 10. In addition, Fig. 11 shows the plan-view contours of the lobes resulting from each experiment, as digitized from the photographs obtained.

From the five experimental videos recorded, the elapsed time for the flows to reach their runout distance is less than 3 s; thus, the calculated average Reynolds numbers of the tailings flows do not exceed 71 in the experiments, which is virtually within the laminar regime. In addition, no vortices or visual evidence of turbulence was observed.

4.3 Numerical Experiments

Table 4 shows a summary of the numerical results obtained, specifically the dimensions of the at-rest liquefied-tailings lobes. Figures 8, 9, 11, 12 present plan-view and cross-section results, respectively, of the numerically simulated lobe calculated using a Newtonian-fluid constitutive rheological model with average density of 1610 kg/m^3 and average viscosity of 2.62 Pa s (i.e., the parameters measured experimentally). It can be seen that, between the physical and numerical results, the agreement is within − 5% and + 14% in length and width, respectively; the local depth measurements are within the same order of magnitude. Because no visual evidence of turbulence was physically observed, these numerical results do not account for possible transient turbulent behavior during the liquefied-tailings flows.

The results of this benchmark problem are specific to laboratory scales. It is foreseen that, upon attempting to adapt this concept to the actual scale of a tailings storage facility problem, the scaling factor would be a fundamental constraint. Indeed, considering that the flow velocity in a real breach release is very high, and that the level of precision required to implement a finite-volume mesh is also high, the computational expense may yield the simulation cost-prohibitive, despite that computational instabilities can be corrected with gradual adjustments of simulation time-step.

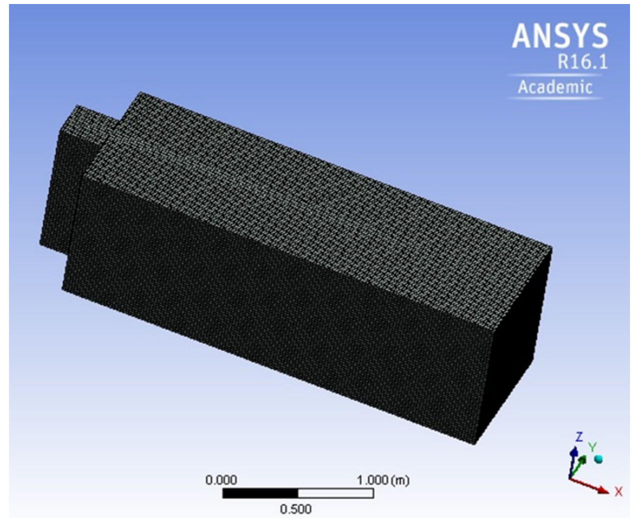

Fig. 7 Numerical model of the flume and tailings container

5 Conclusions

This paper presents a laboratory-scale benchmark case of liquefied-tailings flow. The at-rest shapes of a series of physical experiments of filtered-tailings liquefied-paste flow are compared to those predicted via computational fluid dynamics (CFD) simulations. This benchmark problem will aid numerical research specific to tailings flows. The following major conclusions can be stated:

1. Unlike the initial premise, the liquefied filtered tailings used show essentially zero-yield stress as well as low viscosity (about 2.6 Pa s). Therefore, these liquefied tailings exhibit a practically Newtonian behavior despite its relatively high solid concentration (70% in weight). From a rheological point of view, the behavior

Table 3 Local measurements in the spilled tailings at-rest lobe

Experiment	Length (m)	Width (m)	Depth at the gate (m)	Depth at 30 cm downstream (m)	Depth at the downstream end (m)
1	0.900	0.890	0.048	0.039	0.005
2	0.715	0.800	0.066	0.045	0.013
3	0.690	0.765	0.065	0.047	0.010
4	0.785	0.790	0.054	0.041	0.008
5	0.655	0.723	0.070	0.046	0.012

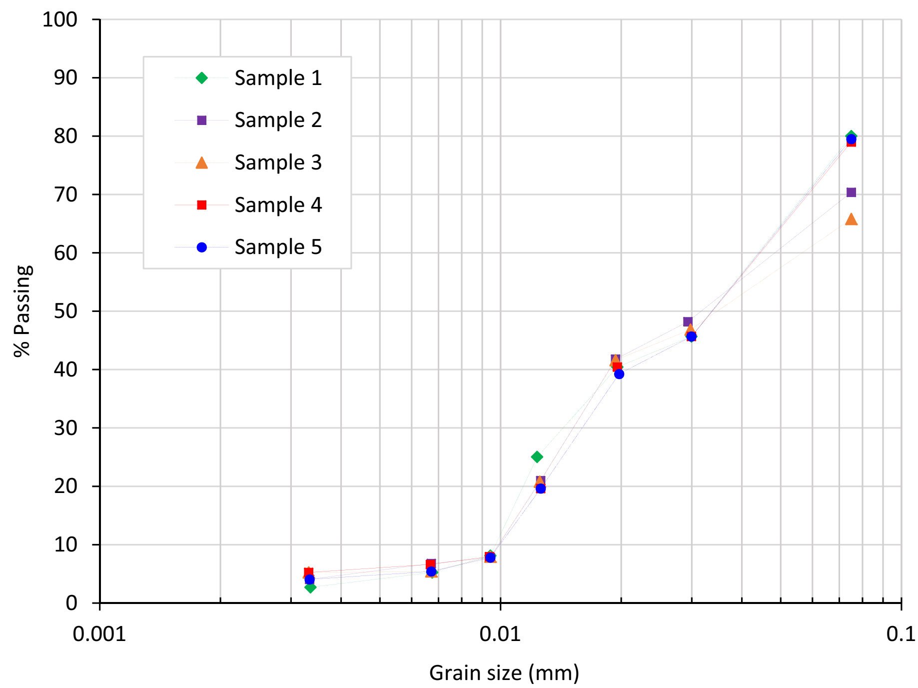

Fig. 8 Grain-size distribution of the tailings used

Table 4 Average dimensions of the at-rest lobes (and coefficient of variation)

Lobe dimension	Physical experiments	Numerical experiments
Length (m)	0.75 (12.9%)	0.71 (5.8%)
Width (m)	0.79 (7.8%)	0.90 (8.6%)
Depth at the gate (m)	0.06 (15.2%)	0.16 (3.5%)
Depth at 30-cm downstream(m)	0.04 (7.9%)	0.06 (0%)
Depth at the downstream end (m)	0.01 (33.4%)	0.04 (0%)

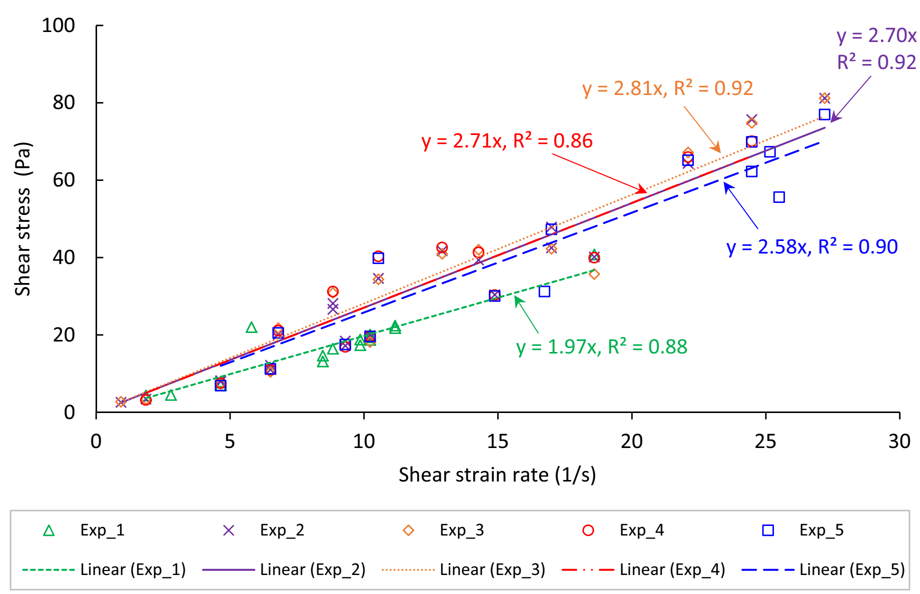

Fig. 9 Flow curves of the liquefied tailings, fitted to Newtonian rheological models

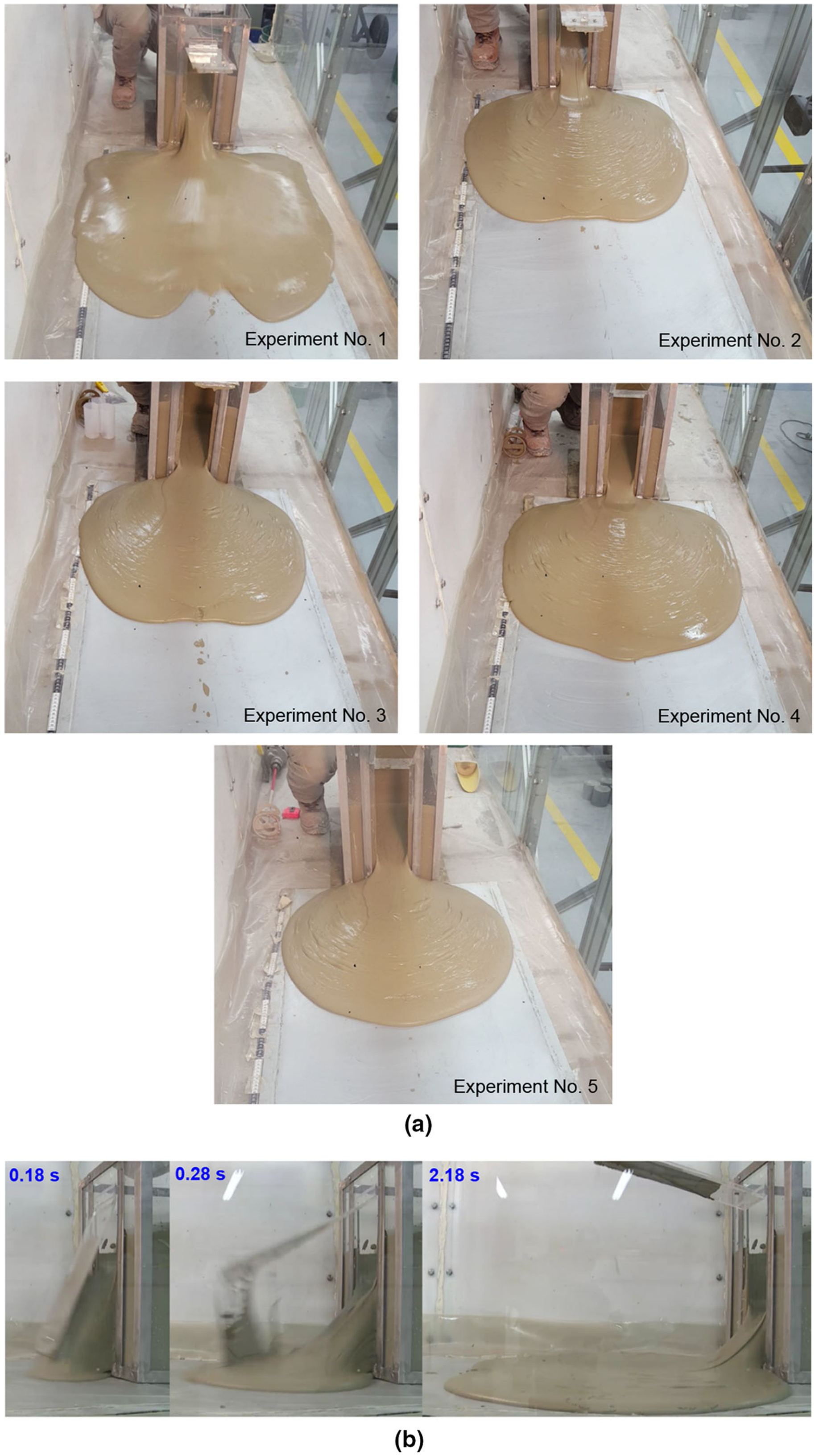

Fig. 10 Footprints (lobes) resulting from the benchmark experiments. **a** Appearance of the lobes; **b** still images from side-view high-speed video

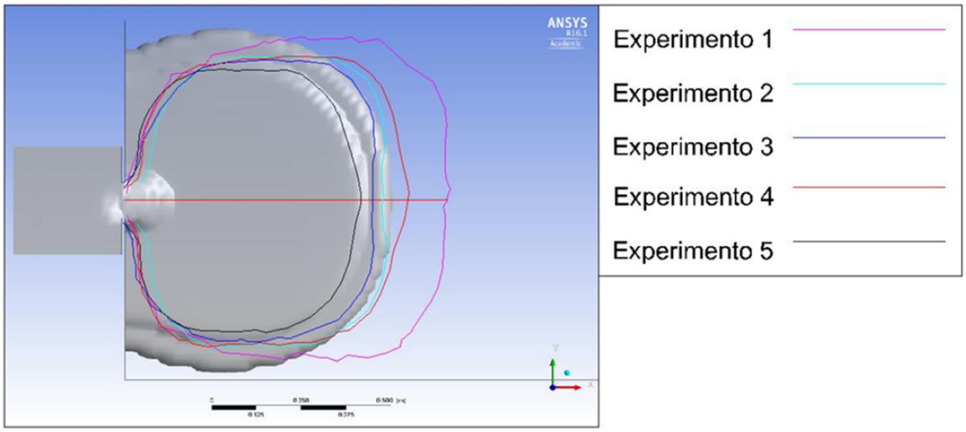

Fig. 11 Plan-view comparison of the flow lobes: the five physical experiments vs. the numerical experiment with average density and viscosity

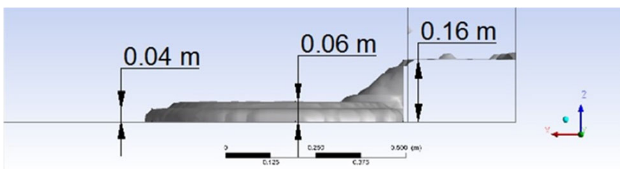

Fig. 12 Cross section of the at-rest flow lobe, obtained numerically with average density and viscosity

of a filtered-tailings paste can be attributed not only to its mineral signature, but also to the possible loss of clay minerals in the tailings because of in-plant filtering dewatering. The absence of clay fraction explains the virtually zero value of yield stress in the liquefied tailings.

2. The use of a Navier–Stokes model, approximated using the CFD finite-volume VOF technique, simulates well the at-rest shape of a liquefied-tailings flow at laboratory scale (the physical and numerical results agree within − 5% and + 14% in length and width of the at-rest lobe, respectively). In this study, the physical parameters measured in the laboratory were used as input values for the numerical simulations. However, this study does not account for transient turbulent behavior during liquefied-tailings flow.

Acknowledgements Pontificia Universidad Javeriana (Vicerrectoría de Investigación) provided partial support for this research through the research Grant No. 6575. The Department of Civil Engineering of Pontificia Universidad Javeriana also provided partial support. The sponsors had no involvement in study design; in the collection, analysis, and interpretation of data; in the writing of the report; or in the decision to submit the article for publication. The authors are also grateful for the support of Dr. Diego Cobos from Dynami Geoconsulting, Colombia, who provided the tailings and valuable technical comments. Likewise, they would like to thank the comments of Dr. Alfonso M. Ramos-Cañón and Dr. Jorge A. Escobar-Vargas of Pontificia Universidad Javeriana, and Dr. Miguel A. Cabrera of Universidad de Los Andes.

References

1. McDermott RK, Sibley JM (2000) The Aznalcóllar tailings dam accident—a case study. Miner Resour Eng 9:101–118. https://doi.org/10.1142/S0950609800000111
2. Rico M, Benito G, Díez Herrero A (2008) Floods from tailings dam failures. J Hazard Mater 154:79–87. https://doi.org/10.1016/j.jhazmat.2007.09.110
3. Santamarina JC, Torres-Cruz LA, Bachus RC (2019) Why coal ash and tailings dam disasters occur. Science 364:526–528. https://doi.org/10.1126/science.aax1927
4. Blight GE, Fourie AB (2005) Catastrophe revisited—disastrous flow failures of mine and municipal solid waste. Geotech Geol Eng 23:219–248. https://doi.org/10.1007/s10706-004-7067-y
5. ICOLD (2001) Tailings Dams—Risk of dangerous occurrences. Lessons learnt from practical experiences—Bulletin 121, International Commission on Large Dams, Paris. ISBN: 9280720538 9789280720532
6. Marr A (2019) Geotechnical aspects of tailings dams & their failures. https://tinyurl.com/Marr-Slides. Accessed 5 Sept 2019
7. Eriksson N, Adamek P (2000) The tailings pond failure at the Aznalcóllar mine, Spain. In: Sixth international symposium on environmental issues and management of waste in energy and mineral production, pp 109–116
8. Zabala F, Alonso EE (2011) Progressive failure of Aznalcollar dam using the material point method. Geotechnique 61:795–808. https://doi.org/10.1680/geot.9.P.134
9. Gens A, Alonso EE (2006) Aznalcóllar dam failure. Part 2: Stability conditions and failure mechanism. Geotechnique 56:185–201. https://doi.org/10.1680/geot.2006.56.3.185
10. Alonso EE, Gens A (2006) Aznalcóllar dam failure. Part 1: Field observations and material properties. Geotechnique 56:165–183. https://doi.org/10.1680/geot.2006.56.3.165
11. Olalla C, Cuellar V (2001) Failure mechanism of the Aznalcollar Dam, Seville, Spain. Geotechnique 51:399–406
12. Alonso EE, Gens A (2006) Aznalcóllar dam failure. Part 3: Dynamics of the motion. Geotechnique 56:203–210. https://doi.org/10.1680/geot.2006.56.3.203
13. Blight GE, Fourie AB (2003) A review of catastrophic flow failures of deposits of mine waste and municipal refuse. In: Introductory report of the international workshop on occurrence and mechanisms of flows in natural slopes and earthfills, IW-FLOWS2003, Associazione Geotecnica Italiana (AGI), Sorrento, Italy, 14–16 May 2003.

14. Morgenstern N, Vick SG, Viotti C, Watts BD (2016) Fundao tailings dam review panel: Report in the immediate causes of the failure of the Fundao Dam, New York
15. Reid D (2019) Additional analyses of the fundão tailings storage facility in situ state and triggering conditions. J Geotech Geoenvironmental Eng 145:04019088. https://doi.org/10.1061/(asce)gt.1943-5606.0002123
16. Hudson-Edwards K (2016) Tackling mine wastes. Science 352:288–290. https://doi.org/10.1126/science.aaf3354
17. Clayton S, Grice TG, Boger DV (2003) Analysis of the slump test for on-site yield stress measurement of mineral suspensions. Int J Miner Process 70:3–21. https://doi.org/10.1016/S0301-7516(02)00148-5
18. Gao J, Fourie A (2015) Using the flume test for yield stress measurement of thickened tailings. Miner Eng 81:116–127. https://doi.org/10.1016/j.mineng.2015.07.013
19. Julien PY, León CS (2000) Mudfloods, mudflows and debris flows, classification in rheology and structural design. In: Proceedings of the international workshop on the debris flow disaster of December 1999 in Venezuela, Universidad Central de Venezuela, Caracas, Venezuela, p 15
20. Zhang S, Zhang L, Qi Q, Li Q, Shi P (2015) Numerical simulation of the characteristics of debris flow. Int J Heat Technol 33:127–132
21. Nguyen QD, Boger DV (1998) Application of rheology to solving tailings disposal problems. Int J Miner Process 54:217–233. https://doi.org/10.1016/S0301-7516(98)00011-8
22. Versteeg HK, Malalasekera W (1995) An introduction to computational fluid dynamics: the finite method, 2nd edn. Longman Scientific & Technical, Essex
23. Gao J, Fourie A (2015) Spread is better: an investigation of the mini-slump test. Miner Eng 71:120–132. https://doi.org/10.1016/j.mineng.2014.11.001
24. Satpathy K, Velusamy K, Patnaik BSV, Chellapandi P (2011) Numerical investigation of vortex shedding past a finite circular cylinder mounted on a flat plate. Numer Heat Transf Part A Appl 59:882–909. https://doi.org/10.1080/10407782.2011.578012
25. Lin T, Liu GR (2017) A development of a GSM-CFD solver for non-Newtonian flows. Comput Fluids 142:57–71. https://doi.org/10.1016/j.compfluid.2016.09.009
26. Yabusaki SB, Şengör SS, Fang Y (2015) A uranium bioremediation reactive transport benchmark. Comput Geosci 19:551–567. https://doi.org/10.1007/s10596-015-9474-y
27. Mayer KU, Alt-Epping P, Jacques D, Arora B, Steefel CI (2015) Benchmark problems for reactive transport modeling of the generation and attenuation of acid rock drainage. Comput Geosci 19:599–611. https://doi.org/10.1007/s10596-015-9476-9
28. Kramer SL (1996) Geotechnical earthquake engineering. Prentice Hall, Upper Saddle River
29. Robertson PK (2010) Evaluation of flow liquefaction and liquefied strength using the cone penetration test. J Geotech Geoenvironmental Eng 136:842–853. https://doi.org/10.1061/(ASCE)GT.1943-5606.0000286
30. Pastor M, Quecedo M, Fernández Merodo JA, Herrores MI, González E, Mira P (2002) Modelling tailings dams and mine waste dumps failures. Géotechnique 52:579–591
31. Highter WH, Tobin RF (1980) Flow slides and the undrained brittleness index of some mine tailings. Eng Geol 16:71–82. https://doi.org/10.1016/0013-7952(80)90008-3
32. Hungr O (2008) Simplified models of spreading flow of dry granular material. Can Geotech J 1:1–26
33. Hungr O, Mcdougall S (2009) Two numerical models for landslide dynamic analysis. Comput Geosci 35:978–992. https://doi.org/10.1016/j.cageo.2007.12.003
34. Hutter K, Wang Y, Pudasaini SP (2005) The Savage-Hutter avalanche model: How far can it be pushed? Philos Trans R Soc A Math Phys Eng Sci 363:1507–1528. https://doi.org/10.1098/rsta.2005.1594
35. Gheshlaghi ME, Goharrizi AS, Shahrivar AA (2013) Simulation of a semi-industrial pilot plant thickener using CFD approach. Int J Min Sci Technol 23:63–68
36. Chen L, Duan Y, Pu W, Zhao C (2009) CFD simulation of coal-water slurry flowing in horizontal pipelines. Korean J Chem Eng 26:1144–1154. https://doi.org/10.1007/s11814-009-0190-y
37. Jeong SW, Locat J, Torrance JK, Leroueil S (2015) Thixotropic and anti-thixotropic behaviors of fine-grained soils in various flocculated systems. Eng Geol 196:119–125. https://doi.org/10.1016/j.enggeo.2015.07.014
38. Niroshan N, Sivakugan N, Veenstra RL (2018) Flow characteristics of cemented paste backfill. Geotech Geol Eng 36:2261–2272. https://doi.org/10.1007/s10706-018-0460-8
39. Dai Z, Huang Y, Jiang F, Huang M (2016) Modeling the flow behavior of a simulated municipal solid waste. Bull Eng Geol Environ 75:275–291. https://doi.org/10.1007/s10064-015-0735-8
40. Huang Y, Mao W, Zheng H, Li G (2012) Computational fluid dynamics modeling of post-liquefaction soil flow using the volume of fluid method. Bull Eng Geol Environ 71:359–366. https://doi.org/10.1007/s10064-011-0386-3
41. O'Brien BJS, Fullerton WT (1993) Two-dimensional water flood and mudflow simulation. J Hydraul Eng 119:244–261
42. Environmental Protection Agency (1992) Method 1331—Toxicity Characteristic Leaching Procedure. 1311-1–1311-35. https://www.epa.gov/sites/production/files/2015-12/documents/1311.pdf. Accessed 1 July 2017
43. Inc Brookfield Engineering Laboratories (2007) Brookfield digital rheometer model DV-III operating instructions manual. Brookfield Engineering Laboratories, Inc., Middleboro
44. Valencia-Galindo MD, Beltrán-Rodriguez LN, Sánchez-Peralta JA, Tituaña-Puente JS, Trujillo-Vela MG, Larrahondo JM, Prada-Sarmiento LF, Ramos-Cañón AM (2018) A two-dimensional laser-scanner system for geotechnical processes monitoring. In: McNamara et al. (ed) Physical modelling in geotechnics. Taylor & Francis Group, London, pp 865–870
45. Clemente JLM, Snow RE, Bernedo C, Strachan CL, Fourie A (2013) Dam break analysis applied to tailings dams: USSD workshop summary and perspectives. In: 33rd Annual USSD Conference. U.S. Society on Dams, Phoenix, Arizona, pp 273–297
46. Ye T, Mittal R, Udaykumar HS, Shyy W (1999) An accurate cartesian grid method for viscous incompressible flows with complex immersed boundaries. J Comput Phys 156:209–240
47. Wang Y, Su K, Wu HG, Qian ZD (2017) Flow characteristics of large hydropower bifurcation under structure rounding optimization. Int J Civ Eng 15:515–529. https://doi.org/10.1007/s40999-016-0091-5
48. Jeong W, Seong J (2014) Comparison of effects on technical variances of computational fluid dynamics (CFD) software based on finite element and finite volume methods. Int J Mech Sci 78:19–26
49. Environmental Protection Agency (2006) 40 CFR—Part 261.24—Toxicity characteristic. 59–60. https://www.govinfo.gov/content/pkg/CFR-2004-title40-vol24/pdf/CFR-2004-title40-vol24-sec261-24.pdf. Accessed 1 July 2017
50. Li W, Coop MR, Senetakis K, Schnaid F (2018) The mechanics of a silt-sized gold tailing. Eng Geol 241:97–108. https://doi.org/10.1016/j.enggeo.2018.05.014